The Astrophysical Journal, 373:158–168, 1991 May 20

PARSEC-SCALE PENETRATION OF ULTRAVIOLET PHOTONS INTO MOLECULAR CLOUDS: [C II] 158 MICRON MAPPING OF W3, NGC 1977, AND NGC 2023

J. E. Howe,[1] D. T. Jaffe,[1] R. Genzel,[2] and G. J. Stacey[3]

Received 1990 June 25; accepted 1990 November 12

ABSTRACT

We have mapped the spatial distribution of the 158 μm [C II] fine-structure line in the Galactic sources W3, NGC 1977, and NGC 2023. The emission arises from warm (100–300 K), dense ($n_H > 10^4$ cm^{-3}) photodissociation regions at the surface of molecular gas. In all three sources the emission extends over parsec scales or greater. For W3 and NGC 1977, where the UV source–molecular cloud geometry presents us with an edge-on view of the variation of [C II] intensity into the molecular gas, we have constructed two-dimensional models of the [C II] emission which include the effects of gas clumping and scattering by dust on the transport of UV photons. The observed [C II] distribution and intensity is well modeled by a clumpy or filamentary distribution to the molecular gas, with a clump-interclump gas density ratio of 10^2 or more, which allows deep penetration of carbon-ionizing UV photons into the clouds. The penetration of UV into clumped molecular clouds may also explain the extended far-IR continuum emission from these sources. The total luminosity of [C II] emission from a clumpy molecular cloud with adjacent or embedded OB stars can be as much as an order of magnitude higher than the [C II] luminosity of a uniform cloud. In addition, the extended penetration of UV into molecular clouds will affect the abundances of atomic and molecular species and increase the fractional ionization of interclump gas and UV-illuminated clump surfaces.

Subject headings: infrared: spectra — interstellar: matter — nebulae: individual (NGC 1977, NGC 2023, W3)

1. INTRODUCTION

The 157.7 μm $^2P_{3/2} \rightarrow {}^2P_{1/2}$ [C II] fine-structure line has been detected in a number of galactic sources, including H II region–molecular cloud interfaces, reflection nebulae, and the Galactic center (Russell et al. 1980, 1981; Kurtz et al. 1983; Stacey et al. 1983; Crawford et al. 1985; Lugten et al. 1986), and in external galaxies (Crawford et al. 1985; Stacey et al. 1991). It is a major cooling line in regions of atomic and molecular gas with densities and temperatures such that $nT \geq 10^4$ cm^{-3} K. Since neutral carbon has an ionization potential of 11.3 eV, the [C II] line arises in the predominantly neutral gas outside H II regions or near B stars and can trace ultraviolet (UV) photons with energies less than the Lyman limit. An analysis of the ionization and excitation of C$^+$ indicates that dense UV-illuminated interfaces at the boundaries of molecular clouds dominate the global 158 μm [C II] emission from the interstellar medium (Crawford et al. 1985). The strong correlation of [C II] and CO $J = 1 \rightarrow 0$ emission across the Galactic plane supports this view (Stacey et al. 1985).

Compact H II regions are usually embedded within or are adjacent to molecular clouds, with a predominantly neutral atomic region between the ionized gas and the molecular material. In many cases, the molecular gas has a H$_2$ density in excess of 10^4 cm^{-3}. For normal dust-to-gas ratios, the dust mixed with the high-density gas will dominate the absorption of carbon-ionizing photons incident on the H II region–molecular cloud interface (Werner 1970; Walmsley 1975). The UV opacity of the dust results in a thin C$^+$ region at the cloud surface (Zuckerman & Ball 1974; Pankonin et al. 1977). For example, for a molecular hydrogen density of 3×10^4 cm^{-3}, the C$^+$ layer will be ~0.03 pc thick, or about 3″ at the distance of M17 or W3. In regions with edge-on geometries, the C$^+$ zone should be unresolved in typical 40″–60″ diameter beams. In clouds containing embedded compact H II regions, the [C II] emission zone should be only marginally larger than the radio continuum source.

The results of one- and two-dimensional mapping observations of the 158 μm [C II] line do not agree with a simple picture of thin, uniform interfaces on UV-illuminated dense molecular clouds. In both edge-on and embedded regions, the scale length for the drop-off of [C II] emission away from the interface and into the molecular region is 10–100 times larger than expected from uniform gas at densities greater than 10^4 cm^{-3} (Stutzki et al. 1988; Matsuhara et al. 1989; this paper). The resolution of this apparent contradiction lies in the nonuniformity of the gas in the clouds. There is extensive evidence for clumping of molecular gas on scales less than 1 pc in the Rosette cloud (Blitz & Stark 1986) and in other galactic clouds (Perault, Falgarone, & Puget 1985) and on scales less than 0.2 pc in the M17 SW cloud both near the H II region (Stutzki & Güsten 1990) and far from any known heating sources (Genzel 1990). Optical imaging of neutral atomic and low–ionization state gas in regions like Orion A and M8 demonstrate the inhomogeneous nature of the interfaces themselves. The observations show filaments, multiple ionization fronts, and globules of neutral gas embedded in the ionized medium (e.g., Elliot & Meaburn 1974; Münch & Taylor 1974). Radio continuum images of Orion A at a resolution of a few arcseconds reveal a rich complex of filamentary ionization ridges near the Trapezium (Yusef-Zadeh 1990).

Based on the extensive evidence for clumping of the molecular material, Stutzki et al. (1988) show that penetration of UV radiation into the cloud through relatively tenuous interclump gas can explain the spatial extent of the [C II] emission in M17 (scale length >2 pc). The UV flux then produces bright [C II]

---

[1] Department of Astronomy, R. L. Moore Hall, University of Texas at Austin, Austin, TX 78712.

[2] Max-Planck-Institut für extraterrestrische Physik, D-8046 Garching bei München, Germany.

[3] Department of Physics, University of California, Berkeley, CA 94720.

emission on the clump surfaces far into the cloud. The required UV radiation penetration depth is consistent with the observed clump sizes and the volume filling factor of clumps in M17 SW (Stutzki & Güsten 1990). The clumpy structure also explains the similarity of the distribution of C^0, as seen in the 370 μm $^3P_2 \rightarrow {}^3P_1$ transition, with $C^{18}O$ $J = 2 \rightarrow 1$ emission which originates in dense clumps (Genzel et al. 1988).

A discussion of the distribution and intensity of the [C II] line beyond simple scale-length arguments must make use of detailed models of the energetics and photochemistry of photodissociation regions (PDRs) along the edges of molecular clouds. In the standard model of Tielens & Hollenbach (1985a, hereafter TH), a far-UV flux G of 10^5 G_0 ($G_0 = 1.7 \times 10^{-3}$ ergs s^{-1} cm^{-2}, the UV flux of the mean interstellar radiation field) impinges on a molecular cloud of hydrogen nucleus density $n_H = 2 \times 10^5$ cm^{-3}. Up to a visual extinction $A_V \sim 2$, energetic electrons photoejected from dust grains are the primary heating source for the gas, and the gas temperature can exceed the dust temperature. [C II] is a major coolant up to $\sim A_V =$ 2–3 in this model, corresponding to a hydrogen column density $N_H \sim 4\text{–}6 \times 10^{21}$ cm^{-2}. At $A_V \sim 4$, the [C II] cooling rate is down by a factor of $\sim$40. The model has successfully predicted the emergent intensities of far-infrared fine-structure lines of O^0 as well as C^+ in several sources (e.g., Orion, Tielens & Hollenbach 1985b; NGC 7023, Chokshi et al. 1988). In addition, the model predicted the scaling of [C II] intensity, $I_{[C\,II]}$, with UV flux observed by Crawford et al. (1985) in a large sample of galactic and extragalactic [C II] sources. For the reflection nebula NGC 2023, the PDR models of Black & van Dishoeck (1987) and van Dishoeck & Black (1988) reproduce the fluorescent H_2 spectrum observed at one position in the source as well as the [C II] line intensity.

In this paper, we seek to improve our understanding of the structure and physics of PDRs by presenting and analyzing large-scale maps of the 158 μm [C II] emission from three galactic sources: W3, NGC 1977, and NGC 2023. The far-infrared (FIR) luminosities of the sources vary from a few 10^3 $L_\odot$ to $\sim 10^6$ $L_\odot$, and the local interstellar UV radiation field ranges from several 10^2 G_0 to a few 10^5 G_0. Two of the sources, W3 and NGC 1977, present very favorable geometries for studying the penetration of the [C II] emission region into dense molecular gas. We consider for these sources the viability of a uniform medium at the interface and investigate several schemes for modeling the penetration of UV radiation into clumpy clouds, as well as the effect of the UV on the excitation of atomic interfaces. We will use the modeling results to draw conclusions about the means by which the UV penetrates a molecular cloud, the structure of the PDRs, the nature of the interclump medium, and the global brightness of [C II] emission.

2. OBSERVATIONS AND DATA ANALYSIS

We observed the [C II] line with the University of California–Berkeley Mk II tandem Fabry-Perot spectrometer (Lugten 1987) on the NASA Kuiper Airborne Observatory on three flights in 1988 January. On these flights the spectrometer contained a three-element linear array of stressed Ge:Ga detectors in place of the previous single stressed detector (Stacey et al. 1991). The beam shape from the instrument is approximately Lorentzian with a spatial resolution of 55″ full width at half-maximum intensity (FWHM) for each detector and a solid angle on the sky of $\Omega_B = 8.6 \times 10^{-8}$ sr. The beam center spacing for the detector array is 55″, as determined by observations of Jupiter. The spectral resolution is 67 km s^{-1} for the center detector and 91 km s^{-1} for the side detectors. The telescope secondary chopped at 33 Hz with a chop amplitude of 5′–6′.

The data were calibrated by observing an internal blackbody source before each mapping series. We referenced the blackbody source in flight to a 150 μm observation of Jupiter (3.1×10^5 Jy: Loewenstein et al. 1977; Hildebrand et al. 1985). The system noise-equivalent power (NEP), including all atmospheric and instrumental losses, was $\sim 4 \times 10^{-15}$ W $Hz^{-1/2}$. We estimate the absolute calibration accuracy for the observations to be ±30%. The point-to-point calibration uncertainties in the maps are much better; a conservative estimate is ±5%. The positional accuracy of the maps is about ±15″, or one-fourth of a beam diameter.

To map each source, the telescope rastered automatically through a rectangular grid of positions. The observations for a 36 point map took $\sim$7 minutes. The normally scanning Fabry-Perot etalon was fixed at the [C II] line center, and the data were integrated for 5–10 s per mapping position with the beam chopping between the map position and a reference position off the source. The [C II] line is unresolved for all the sources. For the central region of W3, we made a second set of raster scans with the etalon tuned off the [C II] line to provide a map of the 158 μm continuum emission. To aid in calibrating the maps, we took double-beamed (that is, chopping symmetrically on either side of a source) spectral scans at the FIR peaks in each source. We could then check for instrumental offsets in our single-beam mapping data by comparing to the spectral scans.

Unless otherwise noted, the point spacing for the maps is 60″. The resulting grid of observed points deviates somewhat from uniform spacing because of field rotation and random ($\sim$5″ rms) point-to-point positioning errors during the automated telescope rastering. We generated contour maps by regridding the data on an evenly spaced grid using a conical interpolation, weighting with an interpolation radius of 72″. The final contour map resolution is $\sim$80″ in all figures except Figure 3, which is fully sampled on a 30″ grid and has a resolution $\sim$60″. The peak pixel values in the maps are less than the actual intensities we observed in our 55″ beam because of the smoothing introduced by the regridding process. The contour levels in the maps are relative to the smoothed map peak pixel value (given in the figure captions) rather than to the peak intensities in a 55″ beam (Table 1).

Since [C II] emission is sometimes extended on scales larger than the 5′–6′ chopper throw, the maps are corrected for emission in the reference beam. For W3, the chopper throw was 4ʹ.7 with the reference beam to the east. We took a series of spectral scans at 5′ spacing from 5′ west to 15′ east of IRS 5, placing the source beam onto the position of the previous reference beam. We then reconstructed the true [C II] and 158 μm continuum distribution along this cut, assuming no emission 15′ east of IRS 5. The rastered mapping data was then corrected for emission in the reference beam using the calibrated line and continuum intensities indicated by the spectral scan cut. The peak intensities of the calibrated W3 mapping data agree with the corrected cut peak intensities to better than 10% for the line maps and 15% for the continuum map. The W3 map scale is 0.7 pc $arcmin^{-1}$. The data set for Figure 1, which shows the [C II] distribution for a 55 $arcmin^2$ area of W3, includes three sets of 60″ spaced observations and, for the inner 5′ × 3ʹ.5 centered at IRS 5, a set of 30″ spaced observations. The 158 μm

1991ApJ...373..158H

TABLE 1

SOURCE PROPERTIES

Source	Peak $I_{[\mathrm{C\,II}]}$ [a] (ergs s^{-1} cm^{-2} sr^{-1})	L_{FIR} ($L_\odot$)	$L_{[\mathrm{C\,II}]}$ ($L_\odot$)	Δv [b] (km s^{-1})	T_B [c] (K)	$N_{\mathrm{C^+}}$ [d] (cm^{-2})	References
W3	2.88×10^{-3}	10^6	1530	6.7	100	1.3×10^{18}	1, 2
NGC 1977	2.03×10^{-3}	4000	34	1.1–1.9	190–310	8.8×10^{17}	3, 4
NGC 2023	1.05×10^{-3}	2100	6.9	1.5–2.0	110–140	4.6×10^{17}	5, 6, 7

[a] Maximum integrated 158 μm [C II] intensity observed in a 55″ beam.

[b] Line widths based on radio observations of carbon recombination lines.

[c] Planck brightness temperature estimated using line widths of the previous column.

[d] Minimum column density of C^+ at position of peak $I_{[\mathrm{C\,II}]}$.

REFERENCES.—(1) Thronson, Campbell, & Hoffman 1980; (2) Jaffe & Wilson 1981; (3) Makinen et al. 1985; (4) Kutner et al. 1985; (5) Emerson, Furniss, & Jennings 1975; (6) Knapp, Brown, & Kuiper 1975; (7) Pankonin & Walmsley 1978.

continuum emission (Fig. 2) has been subtracted from the inner 5′ × 5′ of the W3 [C II] maps. Outside this region the 158 μm continuum radiation contributes at most 15% of the flux in the line maps. Figure 3 shows the distribution of 158 μm [C II] in the central 5′ × 3′.5 of W3. The observations are nearly fully sampled in this region, so the map resolution is ~60″.

For NGC 1977, where the chopper throw was 6′ with the reference beam to the southwest, we have assumed that the northeast corner of the mapped area is free of emission. In Figure 4, we show the distribution of 158 μm [C II] in a 58 arcmin^2 area of NGC 1977, where the map (0, 0) corresponds to a peak in 100 μm continuum emission (Makinen et al. 1985). The NGC 1977 map scale is 0.13 pc arcmin^{-1}. The 158 μm continuum emission from NGC 1977 contributes less than ~5% to the total flux at each position.

For NGC 2023, where the chopper throw was 5′.7 with the reference beam to the west, we assumed the southwest corner of the map to have no emission. Figure 5 shows the [C II] distribution in NGC 2023 for a 51 arcmin^2 region centered at the position of HD 37903. The linear scale for the NGC 2023 map is 0.14 pc arcmin^{-1}. The 158 μm continuum emission from NGC 2023 contributes less than 10% to the total flux.

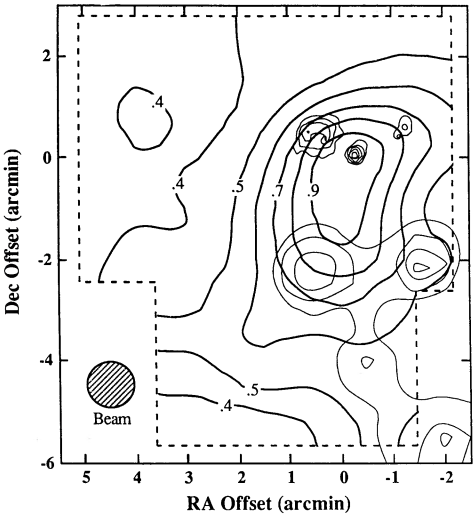

FIG. 1.—The integrated 158 μm [C II] distribution in W3. (0, 0) is at the position of IRS 5 [R.A. (1950) = $02^h21^m53^s.2$, Decl. (1950) = +61°52′21″]. The contour levels range from 0.4–0.9 of the peak map intensity 2.21×10^{-3} ergs s^{-1} cm^{-2} sr^{-1} in intervals of 0.1. For this map and subsequent maps the dashed border indicates the boundaries of the observations. Thin contours represent the compact and ultracompact H II regions W3(A), (B), (C), and (D) (northern sources from left to right), and sources 7, 6, 2, and 1 of Sullivan & Downes (1973) (southern sources from left to right). The map resolution is ~80″.

3. RESULTS

In this section we describe the major features of the [C II] distribution in the sources and derive the physical parameters of the [C II] emission regions. We discuss each source separately. In Table 1 we list various parameters for each of the three sources, including the observed maximum intensities.

3.1. *W3*

W3 is a high-luminosity ($L_{\mathrm{FIR}} \sim 10^6\ L_\odot$; Thronson, Campbell, & Hoffman 1980) star-forming region at a distance of ~2.4 kpc (Georgelin & Georgelin 1976). It contains ~10 compact H II regions whose exciting stars also contribute to the ionization of C^+ in the surrounding neutral medium. The most luminous of these are W3(A) (IRS 1; $L_{\mathrm{FIR}} \sim 3 \times 10^5\ L_\odot$, diameter ~55″), W3(B) (IRS 3; $L_{\mathrm{FIR}} \sim 1 \times 10^5\ L_\odot$, diameter ~21″), W3(C) (IRS 4; $L_{\mathrm{FIR}} \sim 1 \times 10^5\ L_\odot$, diameter ~8″), and W3(D) (diameter ~28″) (Colley 1980; Werner et al. 1980). The shell-like structure and axial symmetry of the thermal radio emission from these sources are signatures of embedded, ionization-bounded H II regions (Harris & Wynn-Williams

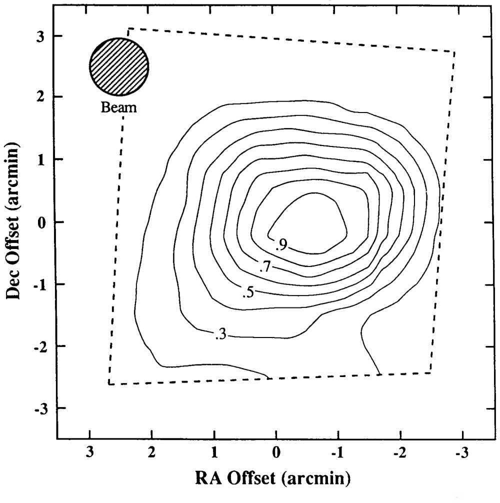

FIG. 2.—The 158 μm continuum in W3. The bandwidth of the continuum observations is 6.7×10^8 Hz. The contour levels range from 0.2–0.9 of the peak map intensity 9.44×10^{-4} ergs s^{-1} cm^{-2} sr^{-1} in intervals of 0.1. The map resolution is ~80″.

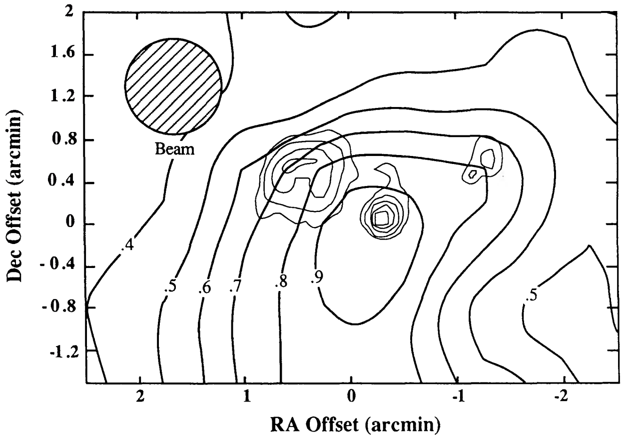

FIG. 3.—The integrated 158 μm [C II] distribution in the central region of W3. The resolution of the map is $\sim 60''$, and the peak map intensity is 2.48×10^{-3} ergs s^{-1} cm^{-2} sr^{-1}. The contour levels range from 0.4–0.9 of the peak map intensity in intervals of 0.1. Thin contours indicate W3(A), (B), (C), and (D).

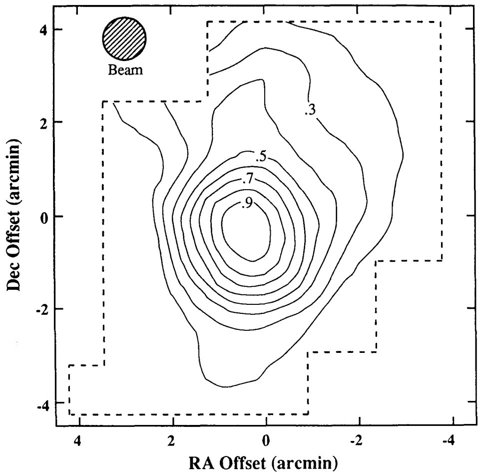

FIG. 5.—The integrated 158 μm [C II] distribution in NGC 2023. (0, 0) is at the position of HD 37903 [R.A. (1950) = $05^{\rm h}39^{\rm m}07^{\rm s}.3$, Decl. (1950) = $-02°16'58''$]. The contour levels range from 0.2–0.9 of the peak map intensity 9.01×10^{-4} ergs s^{-1} cm^{-2} sr^{-1} in intervals of 0.1. The map resolution is $\sim 80''$.

1976; Colley 1980). The bulk of the carbon-ionizing radiation in the W3 molecular cloud, therefore, arises from its interior and not from outside the cloud boundary. The strongest emitter at FIR wavelengths is IRS 5 ($L_{\rm FIR} \sim 2 \times 10^5$ $L_\odot$; Werner et al. 1980), with a luminosity typical of an O6.5 star (Panagia 1973). However, Werner et al. (1980) note that the 15 GHz radio continuum flux toward IRS 5 is more than three orders of magnitude lower than the flux expected from a ZAMS star of this type, and its far-UV flux is not likely to contribute to the production of C$^+$ in the neutral medium.

The large-scale map of W3 (Fig. 1) shows [C II] emission extended over more than 9′ (6 pc), in agreement with the large-beam observations of Melnick et al. (1986). The nominal FWHM of the emission, which is centered near W3(B), is $\sim$3′.5. The emission extends toward W3(C) and W3(D) to the northwest of W3(B), and also extends to the south, with the elongation of the brightest emission somewhat more in the north-south direction than east-west. The 158 μm continuum distribution (Fig. 2) is more compact than the [C II] line distribution and peaks $\sim 15''$ west of the [C II] line emission peak. The continuum intensity drops to 20% of its peak value $\sim$2′.5 from the peak position, in contrast to the [C II] emission, which drops to 20% of its peak $\sim$5′.5 from the center of the emission region.

The [C II] luminosity observed within the mapped region is ~ 1500 $L_\odot$, or about 1.5×10^{-3} of the FIR luminosity (Thronson, Campbell, & Hoffman 1980). A [C II] spectral scan 10′ east of IRS 5 shows that the [C II] line intensity 7 pc from the primary ionizing sources is still nearly 10% of the observed [C II] peak intensity. We do not detect enhanced [C II] emission from W3(A), but the northwest extension of the strongest contour levels indicated a definite contribution from W3(C-D).

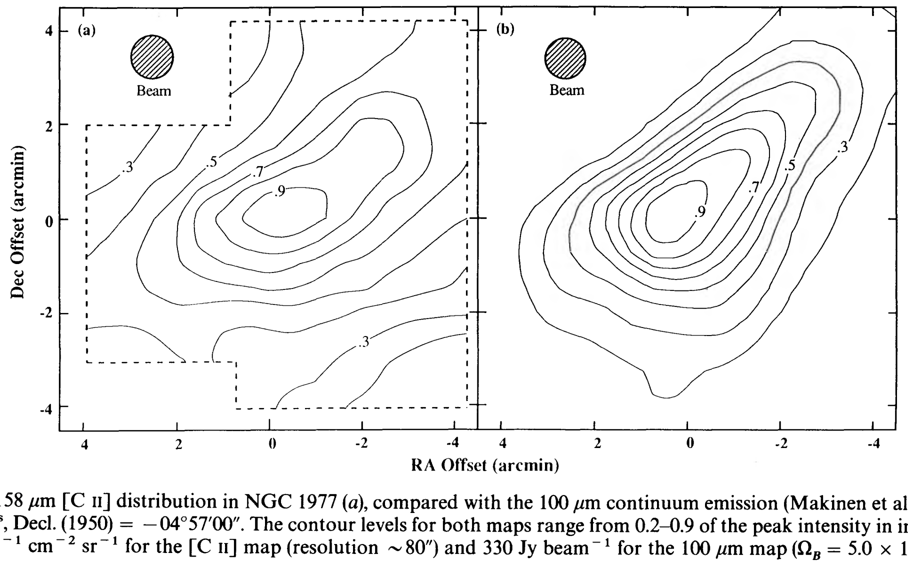

FIG. 4.—The integrated 158 μm [C II] distribution in NGC 1977 (*a*), compared with the 100 μm continuum emission (Makinen et al. 1985) (*b*). The (0, 0) position is at R.A. (1950) = $05^{\rm h}32^{\rm m}44^{\rm s}$, Decl. (1950) = $-04°57'00''$. The contour levels for both maps range from 0.2–0.9 of the peak intensity in intervals of 0.1. The peak map levels are 1.79×10^{-3} ergs s^{-1} cm^{-2} sr^{-1} for the [C II] map (resolution $\sim 80''$) and 330 Jy beam^{-1} for the 100 μm map ($\Omega_B = 5.0 \times 10^{-8}$ sr; resolution $\sim 50''$). 42 Ori is at (2′.8, 4′.8).

The C90α observations of Jaffe & Wilson (1981) show that the region of peak carbon recombination line brightness extends over both W3(A) and W3(B), as well as W3(C-D).

The peak intensity of the [C II] line in our 55″ beam is 2.9×10^{-3} ergs s^{-1} cm^{-2} sr^{-1}. If we assume the 158 μm [C II] line width is similar to the width of the carbon recombination line observed in this source ($\Delta v \sim 6.7$ km s^{-1}; Jaffe & Wilson 1981), we derive a Planck brightness temperature of the [C II] line $T_B \geq 100$ K, where the lower limit corresponds to emission which fills the beam. The Planck brightness temperature gives a lower limit to the excitation temperature for the transition, which is a lower limit to the actual kinetic temperature of the gas. We derive a lower limit to the column density of C^+ at the [C II] emission peak, $N_{C+} \geq 1.3 \times 10^{18}$ cm^{-2}, where we assume the emission is optically thin, the fractional population of the upper state of the C^+ ion is ∼0.5 (appropriate for thermalized gas at a temperature of 200 K), and the beam area filling factor is unity. If the [C II] line is optically thick, the column density will be larger than the lower limit we derive. If we assume the standard cosmic abundance ratio [C]/[H] = 3×10^{-4}, and all of the carbon in the emitting region is ionized, we derive a hydrogen column density $N_H \geq 4 \times 10^{21}$ cm^{-2}, in agreement with column densities predicted from PDR models. The hydrogen gas mass in the [C II]–emitting region is greater than 840 $M_\odot$.

The central [C II] region is associated with dense molecular material. Observations of submillimeter continuum and millimeter transitions of ^{13}CO imply densities of 5×10^4–3×10^5 cm^{-3} (assuming unity volume filling factors) averaged over a roughly 30″ diameter region about IRS 5 (Dickel 1980; Jaffe et al. 1983; Thronson 1986; Hayashi, Kobayashi, & Hasegawa 1989). If we assume an average density of $\sim 10^4$ cm^{-3} for the core region encompassed by the 40% [C II] emission contour, we derive a column density $N_H \sim 4 \times 10^{22}$ cm^{-2} ($A_V \sim 20$) for a column of gas between the [C II] emission peak and the 40% contour (a distance of 1.3 pc) in the direction across our line of sight to W3, a factor of 10 larger than predicted by the one-dimensional PDR models for the total extent of the [C II] region.

The extended spatial distribution of [C II] emission requires carbon-ionizing UV photons throughout the [C II] emission region. If the UV responsible for the extended diffuse [C II] emission emanates from a population of widely distributed early B stars embedded in a uniform density gas (e.g.. B3 stars and a gas density $\sim 10^4$ cm^{-3}), roughly 150 early B stars are required within the central 6 pc of W3 to produce a smooth distribution of [C II] at an intensity comparable to the observed extended emission level of $\sim 1 \times 10^3$ ergs s^{-1} cm^{-2} sr^{-1}. The required number of early B stars is at least twice as high as the number predicted by the (somewhat uncertain) initial mass function for high-mass stars (e.g., Scalo 1986). Although a cluster containing 150 early B stars cannot be ruled out by luminosity considerations, the mass of these stars *alone* would be ∼0.15 of the total mass of the entire W3 cloud complex ($M \sim 10^4$ $M_\odot$; Lada et al. 1978). We therefore consider it unlikely that a widely distributed population of embedded B stars is the source of the extended UV in the W3 cloud.

3.2. *NGC 1977*

NGC 1977 (distance ∼450 ± 60 pc; Genzel et al. 1981; Anthony-Twarog 1982) is an ionization front at the northern edge of the Orion molecular cloud OMC-2. The nearly edge-on geometry of the H II region–molecular cloud interface (Makinen et al. 1985) makes it ideal for a study of the structure of the PDR. The region has been extensively mapped in millimeter rotational lines of CO and its isotopic variants ^{13}CO and $C^{18}O$ (Kutner, Evans, & Tucker 1976; Wootten et al. 1983; Kutner et al. 1985), 2 mm H_2CO lines (Kutner, Evans, & Tucker 1976), 2 and 6 cm carbon recombination lines (Kutner et al. 1979), and 6 cm continuum from the VLA (Kutner et al. 1985), as well as near- and far-IR continuum emission (Makinen et al. 1985) and 610 μm [C I] line emission (Wootten et al. 1982). Makinen et al. conclude that the B1 V star 42 Ori ($L \sim 2.9 \times 10^4$ $L_\odot$; Makinen et al. 1985), which lies ∼3′ to the northeast of the cloud edge, dominates the energetics of the region. 42 Ori is also most likely the sole or principal source of carbon-ionizing UV photons. Although Makinen et al. detected several embedded 2 μm sources, the 2 μm fluxes together with VLA radio continuum measurements place an upper limit later than ∼B3 to the source main-sequence spectral types. Density estimates for the molecular gas range from 10^4 cm^{-3} to 10^6 cm^{-3} (Kutner, Evans, & Tucker 1976; Wootten et al. 1982; Kutner et al. 1985), but there is some question as to whether the density increases or decreases toward the northeast edge of the molecular cloud.

The [C II] emission (Fig. 4*a*) peaks at the 100 μm continuum peak position (Makinen et al. 1985; Fig. 4*b*) and shows a striking similarity to the 100 μm continuum emission. The [C II] contour levels are elongated perpendicular to the direction to the exciting star 42 Ori, which lies 2′.8 east and 4′.8 north of (0, 0). The FWHM of the [C II] emission parallel to the direction to 42 Ori is ∼4′, corresponding to ∼0.5 pc. This is ∼40% greater in extent than the 100 μm continuum FWHM. Observations of CO(3 → 2) emission along a cut extending from 42 Ori through the [C II] emission region show that the edge of the [C II] source is closer to the exciting star than the edge of the CO source (Howe et al. 1990), as expected for a PDR viewed edge-on to the illuminated cloud or clump surface.

The [C II] luminosity within the map of NGC 1977 is ∼34 $L_\odot$, which is 8.5×10^{-3} of the FIR luminosity. The peak surface brightness observed in our 55″ beam is 2.0×10^{-3} ergs s^{-1} cm^{-2} sr^{-1}, which gives a C^+ column density $\geq 8.8 \times 10^{17}$ cm^{-2}. The corresponding hydrogen column density is $\geq 2.9 \times 10^{21}$ cm^{-2}. The hydrogen gas mass of the [C II]–emitting region is ≥ 19 $M_\odot$. If we assume that the width of the 158 μm [C II] line is similar to the 1.1–1.9 km s^{-1} width of the C76α recombination lines in the same region, we derive a brightness temperature $T_B \geq 200$–300 K for the [C II] emission peak. The lower limit to T_B corresponds to emission which fills the beam and has a line-width of 1.9 km s^{-1}.

3.3. *NGC 2023*

The reflection nebula NGC 2023 is excited by the B1.5 V star HD 37903 ($L \sim 2.9 \times 10^4$ $L_\odot$; derived from photometry data [Lee 1968] and a bolometric correction of −1.92 [Mihalas & Morton 1965]). Various distance determinations place the star at 450–500 pc (Lee 1968; Racine 1968; de Boer 1983), and we adopt a distance of 475 pc. HD 37903 is the only likely source of carbon-ionizing photons in NGC 2023. The low visual extinction toward HD 37903 ($A_V \sim 1$; Lee 1968) shows that this star lies on the near side of the molecular cloud. The extent and shape of the reflection nebula imply that the illuminated edge of the cloud is primarily face-on to the observer. The presence of UV-excited 2 μm H_2 emission (Gatley et al. 1987; Hasegawa et al. 1987) and filamentary, extended red emission attributed to photoluminescent hydrogenated amorphous carbon (Witt & Schild 1988) indicates that the stellar UV excites a PDR at the surface of a molecular cloud. The 2 μm H_2 emission peaks in an arc $\sim 75''$ from HD 37903 which is strongest to the southeast and lies just inside a similar arc structure seen in integrated CO($1 \rightarrow 0$) and CO($2 \rightarrow 1$) emission (Gatley et al. 1987; Jaffe et al. 1990; see also White et al. 1990).

The [C II] peak (Fig. 5) is $\sim 30''$ southeast of HD 37903, and the FWHM of the emission is $\sim 3'$, corresponding to ~ 0.4 pc. The low-level emission, however, extends $\sim 5'$ east-west and $\sim 8'$ north-south (~ 1 pc). The bulk of the [C II] emission arises just inside the shell of fluorescently excited 2 μm H_2 emission mapped by Gatley et al. (1987).

The peak surface brightness we observe is 1.1×10^{-3} ergs s^{-1} cm^{-2} sr^{-1}, roughly half the brightness of the NGC 1977 [C II] emission peak. The total cooling of the [C II] line emission within the region mapped is $\sim 7\ L_{\odot}$, corresponding to $\sim 3.3 \times 10^{-3}$ of the FIR luminosity. The total hydrogen gas mass in the [C II] emission region is greater than 4 $M_{\odot}$. If we assume a line width ~ 1.5–2.0 km s^{-1} for the [C II] line, based on carbon recombination line observations of the same region (Knapp, Brown, & Kuiper 1975; Pankonin & Walmsley 1978), we derive $T_B \geq 115$–140 K for the peak [C II] line emission.

4. DISCUSSION

The [C II] line maps of the NGC 1977, NGC 2023, and W3 molecular clouds reveal extended, partially ionized regions a parsec or more in size. In NGC 1977 and NGC 2023, the [C II] emission extends over ~ 1 pc, while for W3 the extent is greater than 3 pc. The extent of the low-level [C II] emission from NGC 2023 is at least partly due to the externally illuminated face-on (or nearly so) geometry presented along our line of sight over most of the nebula northwest of the arc seen in H_2 and CO emission. However, W3, which has embedded ionizing UV sources, and NGC 1977, which is inclined greater than 70° to the plane of the sky (based on the ratio of the major and minor axes of the [C II] map contours), present us with geometries in which the [C II] distribution traces the extent of partially ionized gas into adjacent molecular gas.

The observed extent of [C II] emission from W3 and NGC 1977 is difficult to reconcile with the expected drop-off of [C II] in uniformly distributed molecular gas. The UV attenuation expected from uniform dense gas ($n > 10^4$ cm^{-3}) would result in a thin shell of [C II] emission less than 0.1 pc in extent at the interface of the NGC 1977 cloud or surrounding the compact H II regions in W3. Special geometries where an externally illuminated uniform cloud is tilted with respect to our line of sight also cannot explain the morphology of the [C II] emission in NGC 1977 (see discussion below, § 4.2). In the following sections we discuss two-dimensional models of W3 and NGC 1977 we have constructed to explain the extent and morphology of the [C II] emission from these sources.

4.1. *Two-dimensional* [C II] *Modeling: Description of the Models*

Our two-dimensional [C II] models of W3 and NGC 1977 treat the gas clouds as slabs viewed face-on by the observer, with internal or external source(s) of 6–13.6 eV UV flux in the plane of the cloud. The slab is divided into an array of square pixels (19 × 19 for NGC 1977, 33 × 37 for W3). At each pixel, the UV flux contributed by each stellar source is calculated using one of several schemes for propagating the UV through the slab, which we discuss in more detail below. We assign a gas density to each pixel and use the PDR models of Wolfire, Hollenbach, & Tielens (1989) to derive $I_{[C\,II]}$ from the UV flux and gas density. Wolfire et al. present revised Tielens & Hollenbach (1985a) PDR models for uniform gas and derive the scaling relation of emergent [C II] intensity as a function of the incident UV flux ($G = 10$–10^6 G_0) and gas density ($n_H = 10^2$–10^6 cm^{-3}). In their model $I_{[C\,II]}$ scales roughly logarithmically with G for $\log G \lesssim \log n_H$ (where G is in units of G_0 and n_H is in cm^{-3}), with $I_{[C\,II]}$ more sensitive to G for $G < 10^3$ G_0. In the regime where $\log G \gtrsim \log n_H$, $I_{[C\,II]}$ is insensitive to variations in G but varies roughly logarithmically with n_H. We assume that at some position along the observer's line of sight to each pixel there is a single PDR which responds to the UV flux from each embedded or external UV source and which completely fills the pixel, as viewed by the observer. In all models, however, we assume the distance from a UV source to a PDR is given by their projected separation. After deriving $I_{[C\,II]}$ at each pixel, we construct a contour map of the emission, smoothing the model contour map to the same resolution as the observed [C II] map.

The scale length for the drop-off of the intensity of [C II] emission with distance from illuminating UV sources will be somewhat smaller in a two-dimensional cloud model than in an equivalent three-dimensional model, since the variation of UV flux across the line of sight is most severe in the plane of the UV source. However, since we do not know the distribution of UV sources along our line of sight in a given cloud, the two-dimensional models provide a means of modeling the emission without introducing ad hoc assumptions about the distribution of UV sources in three dimensions. Our assumption of only one PDR along a given line of sight will tend to underestimate $I_{[C\,II]}$, but this effect most likely is compensated by the decreased intensity of multiple PDRs along a line of sight which are farther from the source of UV than the impact parameter distance of the two-dimensional model. In any case, the models serve to illustrate the effects of clumpiness and scattering in molecular clouds regardless of the choice of spatial dimensionality, and offer the best compromise in lieu of a complete understanding of the geometry and density distribution of the molecular gas.

Measurements of the density of the W3 cloud core from observations of submillimeter continuum and molecular line emission range from $\sim 10^4$ cm^{-3} to several 10^5 cm^{-3} (Dickel 1980; Jaffe et al. 1983; Thronson 1986), with the density falling below $\sim 5 \times 10^3$ cm^{-3} beyond 2′ from IRS 5 (Dickel 1980). We modeled the [C II] emission in W3 using two classes of density models: those with constant density throughout the cloud, ranging from 3×10^2–5×10^5 cm^{-3}, and a model with a density gradient radially decreasing from the position of IRS 5 according to the prescription of Dickel (1980). In the latter model, the density is 5×10^4 cm^{-3} within 0.5 pc of IRS 5 and varies as r^{-2} for $r > 0.5$ pc. The NGC 1977 model densities range from 3×10^3–3×10^5 cm^{-3}, guided by the density determinations of Kutner et al. (1985) and Wootten et al. (1983), and include constant density models as well as two different density gradient models, where the density in one model increases from 3×10^4 cm^{-3} at the cloud edge to 10^6 cm^{-3} 5.′5 into the cloud (Kutner et al. 1985) and in the other model decreases from 10^5 cm^{-3} at the edge to 10^4 cm^{-3} 5.′5 into the cloud (Wootten et al. 1983).

The UV source 6–13.6 eV luminosities are estimated from the spectral classification of the exciting star (the case of 42 Ori for the NGC 1977 model), or from radio continuum observations of embedded H II regions (the case of W3), and are fixed parameters of the models. In the W3 model the location and luminosity of embedded UV sources are determined from the radio continuum maps of Sullivan & Downes (1973) and of Harris & Wynn-Williams (1976). Following Rubin (1968), the flux density of the radio sources is used to derive the flux of ionizing photons from the source, and a ZAMS spectral type (Panagia 1973) is assigned *assuming a single ionizing star*. We estimate that the assumption of a single ionizing star rather than a cluster might underestimate the 6–13.6 eV flux by at most a factor of 2 in an extreme case where the Lyman continuum flux responsible for ionizing an H II region originates in a cluster of ~ 5 lower luminosity stars rather than a single ZAMS O star. The 6–13.6 eV UV flux is calculated by assuming the star is a blackbody at the effective temperature given by Panagia (1973). The assumption of a stellar blackbody spectral energy distribution gives UV flux estimates that are within $\sim 30\%$ of LTE line-blanketed stellar models for early B stars (Kurucz 1979), but for O stars the blackbody UV flux is roughly half (or less) of the flux value estimated from the LTE models. The intensity of [C II] emission, however, is rather insensitive to variations in the UV flux for the large fluxes associated with O stars, so the choice of stellar UV flux distribution should not strongly affect the [C II] models. The sources included in the model are W3(A), (B), (C), (D), and components 1, 2, 6, and 7 of Sullivan & Downes (1973). The sole source of UV in the models of NGC 1977 is the star 42 Ori, which lies 3′ (0.4 pc) in projection from the edge of the molecular cloud as determined by CO($3 \rightarrow 2$) observations. The UV flux at the cloud edge (360 G_0) is derived from the B1V spectral class of 42 Ori and the minimum projected distance of the star from the cloud (0.4 pc at a distance of 450 pc to NGC 1977).

Scattering and absorption by dust dominate the radiative transfer of UV in molecular clouds, although absorption by molecular hydrogen and atomic carbon can also play a role (TH). We consider three models for the propagation of the UV through the slab:

1. *Unclumped gas.*—For uniform unclumped gas, the column density of intervening dust and gas between the model pixel position and the UV source governs the attenuation of the UV. The column density, N_H, is calculated from the model gas density distribution of the slab (either uniform or smoothly varying according to models based on observations of the molecular cloud). The mean intensity of the UV field varies as $r^{-2} \exp(-kA_V)$, where r is the distance through the slab from the pixel to the UV source, $A_V = N_H(\text{cm}^{-2})/(1.9 \times 10^{21})$ is the visual extinction through a column density N_H of gas, and k is a constant that accounts for the scattering and attenuation properties of the dust and gas to the UV photons. Implicit in this calculation is the assumption of a constant dust-to-gas ratio. We adopt $k = 1.8$ from the TH standard model. The total UV flux at each pixel is the sum of the contributions from each UV source.

2. *Opaque clumps of gas.*—We have extended the model of Stutzki et al. (1988), in which the gas is composed of opaque clumps embedded in a less dense medium that does not attenuate the UV, to two dimensions. There are two cases in this model, one in which the interclump medium scatters and redistributes the UV (Stutzki et al. model 1) and one in which there is no scattering of the UV by interclump gas (Stutzki et al. model 2). For the case of UV scattering, the UV flux varies as $r^{-2} \exp(-r/R)$, where r is the distance between the UV source and the position in the cloud and R is a scale length that depends on the volume filling factor Φ_V and diameter D_C of the clumps; $R = D_C/\Phi_V$. The r^{-2} factor accounts for geometric dilution of the UV flux, while the exponential factor accounts for the fraction of UV blocked by foreground clumps. For the case of no UV scattering, the UV is only geometrically diluted and therefore varies as r^{-2}, but the fraction of clumps not already shadowed by foreground clumps varies as $\exp(-r/R)$. In the scattering model, then, all the clumps are illuminated, but with a UV flux that is less intense than the nonscattering model UV flux. In the nonscattering model, the UV flux is more intense, but not all of the clumps are illuminated. The intensity of the [C II] emission declines more rapidly with distance into the nonscattering cloud since $I_{[\text{C II}]}$ is linearly dependent on the fraction of clumps illuminated by UV but only logarithmically dependent on the intensity of the UV field.

3. *Scattering and absorption of UV by dust or clumps.*—In this case we treat each UV source in the model cloud as the central source of a 20 zone radially symmetric cloud. Each zone is composed of UV-scattering–absorbing clumps, which occupy the same area filling factor in each zone. The filling factor of clumps and relative fraction of incident UV flux scattered as opposed to absorbed by the clumps are model parameters which may be varied. The scattering occurs only along the radial direction. The UV flux in each zone is computed for each source, and the resulting ensemble of models is added to generate a two-dimensional map of the UV flux throughout the slab.

After the UV flux distribution in the slab has been calculated for any of the radiative transfer models, the theoretical scaling relation between gas density, UV flux intensity, and emergent [C II] intensity of Wolfire, Hollenbach, & Tielens (1989) is applied to each pixel (assuming a beam filling factor of unity for the emitting gas) to generate the distribution of $I_{[\text{C II}]}$. The model contour maps are generated at the same resolution as the regridded observations by applying the same interpolation function used for the observed maps.

4.2. *Two-dimensional* [C II] *Modeling: Model Results*

Figures 6 and 7 show examples of models of W3 and NGC 1977 compared to the observed [C II] maps. Figure 6 compares the observed [C II] distribution in W3 (Fig. 6*a*) to two models. In Figure 6*b* we show a W3 model with $n_H = 10^4$ cm^{-3} in a uniform cloud, and in Figure 6*c* a model of opaque clumps with $n_H = 10^5$ cm^{-3} and a $1/e$ scale length of 2 pc for the UV attenuation (i.e., the volume filling factor Φ_V of clumps with a diameter $D_C = 0.1$ pc would be 0.05, which would attenuate the UV field to $1/e$ of its unblocked value 2 pc from the source of the UV). Figure 7 compares the observed [C II] distribution in NGC 1977 (Fig. 7*a*) to models with density $n_H = 3 \times 10^4$ cm^{-3}. Figure 7*b* is the model for uniform gas, while Figure 7*c* is a clumped gas model with a UV attenuation scale length of ~ 0.4 pc. In the following paragraphs we discuss the general results of the modeling of W3 and NGC 1977 and interpret the model results.

Simple uniform density models fail to explain the observed [C II] *distribution and intensity at any density.*—The [C II] emission in unclumped gas models is confined to a thin layer at the boundary between a source of UV and the molecular cloud. In the case of the W3 models (e.g., Fig. 6*b*), even uniform densities two orders of magnitude or more lower than the molecular densities derived in the central 0.5 pc result in gas

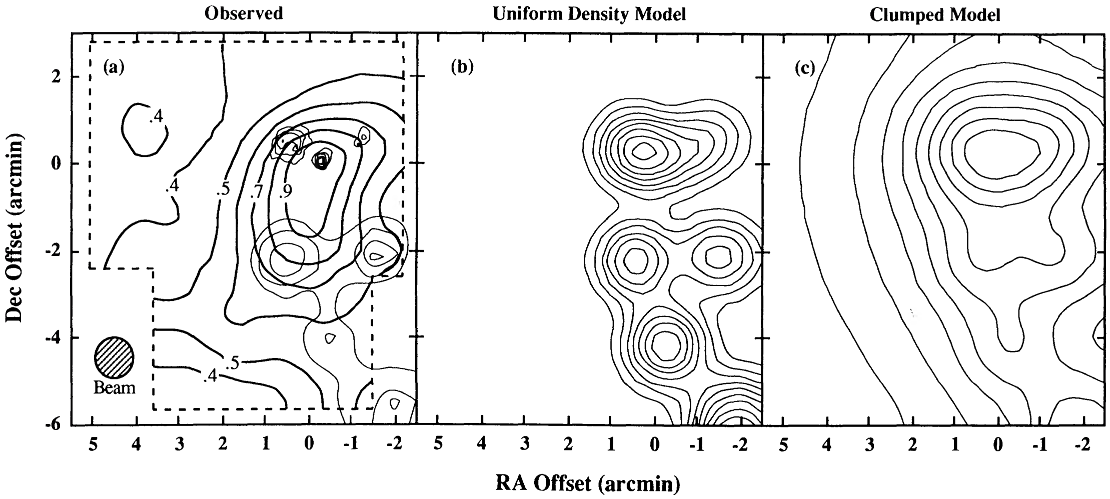

FIG. 6.—Models of the 158 μm [C II] distribution in W3 compared with the observed [C II] distribution. (*a*) Observed [C II] distribution. (*b*) Uniform gas model with $n_H = 1 \times 10^4$ cm^{-3}. The peak intensity is 8.7×10^{-4} ergs s^{-1} cm^{-2} sr^{-1}. (*c*) Clumped gas model with $n_H = 1 \times 10^5$ cm^{-3}, no scattering of the UV by interclump gas, and a scale length of 2 pc to the UV attenuation. The peak intensity is 1.9×10^{-3} ergs s^{-1} cm^{-2} sr^{-1}. Contour levels for the models range from 0.1–0.9 of the peak intensity in 0.1 intervals. The resolution of the model maps is ~80″.

column densities too large to allow sufficient penetration of the UV to excite the [C II] line beyond the inner few arcminutes. In an extreme low-density case for W3 with $n_H = 300$ cm^{-3}, corresponding to $N_H \sim 9 \times 10^{20}$ cm^{-2} pc^{-1}, the UV is able to penetrate to the outer parts of the cloud. However, in this low-density regime, the insensitivity of $I_{[\mathrm{C\,II}]}$ with G (for $G > 10^2\ G_0$) results in a model morphology where the 90% contour is 4 times more extended than the observed 90% contour. In addition, since the upper energy state of C^+ is very subthermally populated at this low density (the ^2P fine-structure level populations of the C^+ ion are not thermalized by collisions with H_2 until $n_{H2} > 5 \times 10^3$ cm^{-3}), the [C II] emission level is down by a factor ~6 from the observed level. The simple uniform gas models for NGC 1977 (e.g., Fig. 7*b*) also fail to reproduce the extent of the penetration of the [C II] emission into the NGC 1977 molecular cloud, as measured from the peak of the [C II] emission southwest into the cloud. Even for a low-density model with $n_H = 3 \times 10^3$ cm^{-3}, the distance from the [C II] peak to the 50% level is 0.45 of observed and to the 30% level is 0.4 of observed. For W3, a model with the density distribution of Dickel (1980) [smoothly varying density with $n_H = 5 \times 10^4\ (r_{\mathrm{IRS\ 5}}/0.5\ \mathrm{pc})^{-2}$, where $r_{\mathrm{IRS\ 5}}$ is the distance in parsecs measured from IRS 5] produces a morphology much more radially symmetric than is observed. Continuous density gradients in the NGC 1977 models also fail to match the observed NGC 1977 morphology.

A simple model for NGC 1977 in which a tilted slab of uniform gas is illuminated by a nearby external source of UV also fails to match the observed [C II] morphology. In this model, the angle of the slab with respect to the plane of the sky is constrained by the observed ratio of the major and minor axes of the [C II] emission contours, which would appear circular if viewed face-on. The tilt angle (the angle between the plane of the slab surface and the plane of the sky) of a uniform slab of gas in this model must be ~65°. This constrains the distance from the cloud surface to the UV source (42 Ori) and

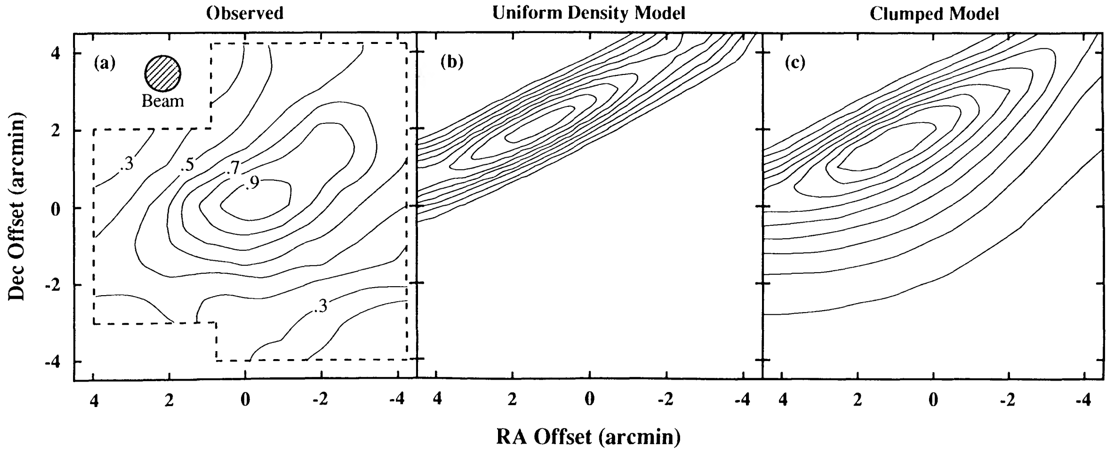

FIG. 7.—Models of the 158 μm [C II] distribution in NGC 1977 compared with the observed [C II] distribution. (*a*) Observed [C II] distribution. (*b*) Uniform gas model with $n_H = 3 \times 10^4$ cm^{-3}. The peak intensity is 6.0×10^{-5} ergs s^{-1} cm^{-2} sr^{-1}. (*c*) Clumped gas model with $n_H = 3 \times 10^4$ cm^{-3}, no scattering of the UV by interclump gas, and a scale length of 0.4 pc to the UV attenuation. The peak intensity is 3.6×10^{-4} ergs s^{-1} cm^{-2} sr^{-1}. Contour levels for the models range from 0.1–0.9 of the peak intensity in 0.1 intervals. The resolution of the model maps is ~80″.

allows one to calculate the variation of UV intensity across the foreshortened slab surface. The apparent morphology of the [C II] emission at the surface of the slab, predicted from PDR models (e.g., TH), is more than twice as extended as the observed emission, regardless of the density of the gas or the intensity of the UV flux. We conclude that the [C II] emission from NGC 1977 is not produced at the surface of a molecular cloud, but traces the extent of ionized carbon into molecular gas. For both W3 and NGC 1977, cloud models with uniformly distributed gas can not reproduce the observed extent of partially ionized gas.

Clumpy cloud models can fit the observed morphology of both W3 and NGC 1977 and, when they do, give reasonable values for the absolute [C II] *intensities.*—The best W3 model fits (e.g., Fig. 6*c*) were obtained in models that diluted the UV flux with a scale length of 2′–3′ ($\sim$1.5–2 pc, corresponding to $\Phi_V \sim$ 0.05–0.07 for $D_C = 0.1$ pc). None of the W3 models with a constant density $\leq 3 \times 10^4$ cm^{-3} for the clumps reproduced the observed dimensions of the 60% contour level in either the north-south or east-west extent to within 20% (our criterion for an acceptable fit). Even though the clump models were adjusted only to match the observed morphology, they also match the observed absolute intensity of the [C II] emission quite well. In general, the absolute intensities of the W3 model maps are close to the observed intensity; $\sim$80% for models with $n_H \geq 3 \times 10^4$ cm^{-3} and a factor of 2–4 lower for the lower density models. The results of the W3 models suggest that the observed morphology and brightness of the [C II] emission in W3 is well explained by the TH PDR model if the emission originates from clumps with a density $\sim 10^5$ cm^{-3} and approximately unity beam filling factor. Low-density uniform gas models indicate that an interclump gas density less than or equal to 300 cm^{-3} allows sufficient penetration of the UV from the radio continuum sources in W3 to excite [C II] emission at the map boundaries. The best-fit clumpy models for NGC 1977 in general have scale lengths for UV attenuation of 2′–4′ (0.25–0.5 pc, corresponding to $\Phi_V \sim 0.2$–0.4 for $D_C = 0.1$ pc) with scattering of the UV by interclump gas. Interclump gas densities ≤ 500 cm^{-3} allow the UV to penetrate on scales of this magnitude. Figure 7 compares models with $n_H = 3 \times 10^4$ cm^{-3}; Figure 7*b* is a model for uniform gas, illustrating the severe drop-off of the [C II] emission with depth into the cloud, while Figure 7*c* is a clumped gas model. All of the NGC 1977 models differ from the observed [C II] distribution in their greater extent in the direction along the cloud edge and in their emission peaking closer to 42 Ori. The latter difference is most likely a result of a combination of a slight inclination of the star–cloud edge geometry (Kutner et al. 1985) and uncertainties in the density of the gas near the cloud edge. The absolute intensities of the NGC 1977 models are lower than the observed intensity by a factor of 2.5–3, with the highest intensities for models with clump densities $\sim 10^4$ cm^{-3}.

The extended [C II] *distribution in W3 and NGC 1977 indicates parsec-scale penetration of carbon-ionizing UV photons into the molecular gas, providing an explanation for extended FIR continuum emission.*—In a uniform, dense molecular cloud, UV can penetrate typically less than 0.1 pc before complete absorption by the dust and gas. Since the FIR emission from dust is a result of heating by embedded or nearby UV sources, the extent of FIR emission in a uniform cloud has previously been explained as the result of reradiation of near-IR photons emitted by dust close to the source of UV, which then penetrate farther into the cloud where they are eventually absorbed by the dust (Scoville & Kwan 1976; Leung 1976; Natta et al. 1981). A clumpy cloud model can explain the extent of the FIR continuum emission as the result of direct absorption of UV by dust without the necessity of absorption of infrared continuum radiation emitted by dust closer to the sources of UV radiation. A feature shared by the [C II] distribution in W3 and NGC 1977 is the greater extent of the [C II] scale length than the FIR continuum scale length. Since in a clumpy cloud the distribution of both the [C II] and the FIR continuum emission is due to direct irradiation by UV, the scale length of the [C II] emission should be greater than that of the FIR continuum since the continuum emission scales directly with G while the [C II] emission varies approximately logarithmically with G.

Scattering of UV has little apparent effect on the [C II] *emission from a clumpy medium.*—The effect of scattering of incident UV in a clumpy medium was also investigated in the models of W3 and NGC 1977, with the result that there was little observable effect in the [C II] distribution. Theoretical models of the scattering effects of dust on UV (Flannery, Roberge, & Rybicki 1980; Roberge, Dalgarno, & Flannery 1981) indicate that the most reasonable fits to the observed extinction of starlight through diffuse clouds are obtained with dust scattering models with dust albedos of $\sim$0.5 and which backscatter only a few percent of the incident UV. The clump densities required by the two-dimensional [C II] models are high enough that clumps of diameter $\sim$0.1 pc are essentially opaque, and almost all incident UV is absorbed by the clumps with only a few percent scattered away. The small increase in G in a clumpy cloud model when scattering is introduced has little effect on the regions of brightest [C II] emission, since for high G the [C II] intensity is insensitive to variations in G, but is more noticeable in the regions of the cloud with little [C II] emission since $I_{[\mathrm{C\,II}]}$ is a stronger function of G when G is small. Even isotropic scattering of the UV by dust with comparable albedo does not significantly change either the intensity or the morphology of the [C II] emission.

The density contrast between clump and interclump gas must be large.—The interclump gas in W3 and NGC 1977 must have a density less than or equal to 300–500 cm^{-3} to explain the extent of the UV penetration if the gas-to-dust ratio is the same in the clumps and the interclump medium. A density of 300–500 cm^{-3} corresponds to $A_V \sim 0.5$–0.75 pc^{-1} into the cloud and indicates that the UV would not be redistributed in angle until it has traversed a distance of a few parsecs in the cloud. The models generally require high clump densities, of order 10^4–10^5 cm^{-3}, to match the observed morphologies and intensities. In W3, all models with $n_H \leq 3 \times 10^4$ cm^{-3} failed to reproduce the observed [C II] distribution, while in NGC 1977 a high density is required to explain the observed intensity of the [C II] emission. If the clumps are in pressure equilibrium with the interclump gas, the estimated brightness temperature of the [C II] emission from clump surfaces ($\sim$100 K) requires the interclump gas temperature to be of order 10^4 K. The maximum temperature predicted by PDR models of low-density gas is $\sim$200 K (Wolfire, Tielens, & Hollenbach 1990), so other heating mechanisms in addition to irradiation by UV are probably necessary to maintain such a high interclump gas temperature. If, however, the assumption of equal gas-to-dust ratios in the clump and interclump gas is relaxed, the required density contrast between the clumps and the interclump medium may be reduced (Genzel 1990), with a corresponding reduction in the interclump gas temperature if the cloud is in pressure equilibrium. Observations of the UV continuum emission from a variety of sources show significant variation in the relative strength of the extinction "bump" at ~2200 Å toward several sources, including θ^1 Orionis (Savage 1975), which may indicate differences in the UV extinction properties of dust in regions of high UV flux. In particular, models of interstellar dust that include polycyclic aromatic hydrocarbons (PAHs) as one of several dust components show that destruction of PAHs in hard UV radiation fields such as those near O stars can significantly decrease the UV absorption cross section of the dust per H nucleon (Désert, Boulanger, & Puget 1990). The significance of the contribution to the UV extinction by PAHs in the interclump medium of molecular clouds then becomes an important issue.

The total cooling in the [C II] *line is greater in a clumpy medium than in a uniform medium.*—A major consequence of the extended penetration of UV into a clumpy medium as opposed to a uniform medium is the enhancement of the total cooling in the [C II] line emission. Although the total UV luminosity deposited in a clumpy cloud is identical to the luminosity deposited in a uniform cloud, the total luminosity emitted in the [C II] line is much greater for a clumpy cloud than for a uniform cloud because of the greater efficiency of the conversion of UV flux into [C II] line emission when G is small. Extended penetration of UV allows geometric dilution of the UV flux density prior to absorption by a clump, thereby increasing the overall efficiency of the [C II] emission mechanism. Models of the [C II] emission from W3 and NGC 1977 indicate the [C II] luminosity can be as much as an order of magnitude greater in clumpy clouds than in uniform density clouds. For example, in models of W3 the flux of [C II] emission integrated over the $8' \times 9'$ area of the model clouds is 11 times greater in a clumpy cloud with a clump density of 10^5 cm^{-3} and a $1/e$ scale length of 2 pc to the attenuation of UV by clumps than in a uniform density cloud, while this factor is ~7 if the density is decreased to 10^4 cm^{-3}. The extended penetration of UV through molecular clouds explains the correlation between the global [C II] emission from galaxies observed by Crawford et al. (1985) with the *average* UV energy density derived from the FIR luminosity of a galaxy and its FIR source size.

5. CONCLUSIONS

The extended [C II] emission in W3 and NGC 1977, together with our modeling results, leads to a picture of molecular clouds as an inhomogeneous medium where UV photons from nearby and embedded OB stars penetrate on greater than parsec scales. The UV shines through relatively tenuous interclump gas and illuminates high-density clumps or filaments, exciting atomic and molecular emission lines from PDRs at the clump surfaces. The clumps or filaments are most likely moving with velocities of a few km s^{-1} with respect to the mean cloud velocity. In M17 there is direct evidence that the clumps have peculiar velocities of 2–5 km s^{-1} (Stutzki & Güsten 1990; see also Martin, Sanders, & Hills 1984). Clump motion in sources like W3 may also cause the large observed molecular line widths. We examine several general consequences of the picture developed from our observations.

Observationally, the penetration of UV into a clumpy cloud implies that not only [C II] but also [C I] and [O I] fine-structure lines should be found deeper into the cloud than expected in a uniform molecular cloud. For clump densities ~10^5 cm^{-3}, the PDR models of TH indicate 63 μm [O I] emission from clump surfaces more than an order of magnitude brighter than the 158 μm [C II] emission for $G > 10^4\ G_0$, and about an order of magnitude brighter for $G \sim 10^3\ G_0$. The [C I] emission will be weak (less than ~10^{-2} of the 158 μm [C II] intensity) but somewhat more extended than [C II] because of the insensitivity of the [C I] emission to the UV flux for $10^3 < G/G_0 < 10^6$.

Clumping not only allows direct UV heating deep into molecular clouds, but also increases the mass fraction of gas in PDRs, since the surface-to-volume ratio is greater for an ensemble of clumps than for a single cloud of equal mass. Photochemical effects, such as an increase in the abundance of C^0 and C^+ relative to CO and possible variations in the CO isotopic ratios due to differing amounts of self-shielding (van Dishoeck & Black 1988), are important throughout a clumpy molecular cloud. Since the clumps are also moving around within the molecular cloud, the changing UV illumination of clumps as they are intermittently shadowed by intervening clumps may increase the importance of nonequilibrium chemical phenomena, since the time scales for shadowing may be comparable to chemical equilibrium time scales. For example, a 0.1 pc diameter clump moving with a projected relative speed of ~5 km s^{-1} across the line of sight from a nearby clump of similar size to a nearby O or B star will shadow the clump for ~2×10^4 yr, roughly comparable to the formation time scale of H to H_2 on the unilluminated clump surface for a clump density of ~5×10^4 cm^{-3} (Graedel, Langer, & Frerking 1982). The nonequilibrium chemical effects may be more noticeable for the case of a single UV source or a few UV sources at a single location illuminating a nearby molecular cloud, since shadowing imparts only a minor perturbation on the UV flux intensity from spatially distributed UV sources. Clumpy molecular clouds, even far from embedded or adjacent OB stars, should be significantly more active photochemically than uniform dark clouds and also more active than one would naively expect based on a picture of smoothly distributed gas.

The ionization fraction in the interclump medium and in the UV-illuminated clump surfaces will be at least 10^{-4} (assuming complete ionization of all species with ionization potentials less than 13.6 eV), roughly 3 orders of magnitude greater than in regions unaffected by UV illumination (Langer et al. 1978; Guélin, Langer, & Wilson 1982; Wootten, Loren, & Snell 1982). In a clumpy cloud threaded by a magnetic field of sufficient strength, there are several consequences of increasing the ionization state of the interclump gas and the clump surfaces which may affect the dynamics of clump collapse and star formation. The partially ionized clump surfaces may resist collapse because of drag induced by charged species tied to magnetic field lines, resulting in a smaller mass fraction of a clump actually forming a star and, therefore, a lower star formation efficiency in the cloud as a whole. The transfer of angular momentum from clump rotation to the interclump gas will also be more efficient since a greater fraction of particles in the interclump medium will follow the motion of the magnetic field lines tied to the clumps. In addition, the kinetic energy of clump motions can provide a means of increasing the thermal energy, and hence the pressure, of interclump gas through Alfvén and magnetosonic waves generated as the clumps move through the partially ionized interclump medium.

We thank the ground and flight crews of the NASA Kuiper Airborne Observatory for the enthusiastic support which made possible the [C II] observations, and N. Geis and A. Poglitsch for invaluable instrumental and observational assistance. We also thank N. Evans, J. Lacy, and J. Stutzki for helpful comments and critiques of earlier versions of this work. J. E. H. acknowledges support from a NASA Graduate Student Researchers Program fellowship. This research was supported by NASA grant NAG2-419 to the University of Texas at Austin and by a NATO Scientific Affairs Division Collaborative Research Grant.

REFERENCES

Anthony-Twarog, B. J. 1982, AJ, 87, 1213
Black, J. H., & van Dishoeck, E. F. 1987, ApJ, 322, 412
Blitz, L., & Stark, A. A. 1986, ApJ, 300, L89
Chokshi, A., Tielens, A. G. G. M., Werner, M., & Castelaz, M. W. 1988, ApJ, 334, 803
Colley, D. 1980, MNRAS, 193, 495
Crawford, M. K., Genzel, R., Townes, C. H., & Watson, D. M. 1985, ApJ, 291, 755
de Boer, K. S. 1983, A&A, 125, 258
Désert, F.-X., Boulanger, F., & Puget, J.-L. 1990, A&A, 237, 215
Dickel, H. R. 1980, ApJ, 238, 829
Elliot, K. H., & Meaburn, J. 1974, Ap&SS, 28, 351
Emerson, J. P., Furniss, I., & Jennings, R. E. 1975, MNRAS, 172, 411
Flannery, B. P., Roberge, W., & Rybicki, G. B. 1980, ApJ, 236, 598
Gatley, I., et al. 1987, ApJ, 318, L73
Genzel, R. 1990, in Proc. Manchester Conference on Molecular Clouds, ed. R. James & T. Millar, in press
Genzel, R., Harris, A. I., Jaffe, D. T., & Stutzki, J. 1988, ApJ, 332, 1049
Genzel, R., Reid, M. J., Moran, J. M., & Downes, D. 1981, ApJ, 244, 884
Georgelin, Y. M., & Georgelin, Y. P. 1976, A&A, 49, 57
Graedel, T. E., Langer, W. D., & Frerking, M. A. 1982, ApJS, 48, 321
Guélin, M., Langer, W. D., & Wilson, R. W. 1982, A&A, 107, 107
Harris, S., & Wynn-Williams, C. G. 1976, MNRAS, 174, 649
Hasegawa, T., Gatley, I., Garden, R. P., Brand, P. W. J. L., Ohishi, M., Lightfoot, J. F., Hayashi, M., & Kaifu, N. 1987, ApJ, 318, L77
Hayashi, M., Kobayashi, H., & Hasegawa, T. 1989, ApJ, 340, 298
Hildebrand, R. H., Loewenstein, R. F., Harper, D. A., Orton, G. S., Keene, J., & Whitcomb, S. E. 1985, Icarus, 64, 64
Howe, J. E., Geis, N., Genzel, R., Jaffe, D. T., Poglitsch, A., & Stacey, G. J. 1990, in Submillimetre Astronomy, ed. G. D. Watt & A. S. Webster (Dordrecht: Kluwer), 285
Jaffe, D. T., Genzel, R., Harris, A. I., Howe, J. E., Stacey, G. J., & Stutzki, J. 1990, ApJ, 353, 193
Jaffe, D. T., Hildebrand, R. H., Keene, J., & Whitcomb, S. E. 1983, ApJ, 273, L89
Jaffe, D. T., & Wilson, T. L. 1981, ApJ, 246, 113
Knapp, G. R., Brown, R. L., & Kuiper, T. B. H. 1975, ApJ, 196, 167
Kurtz, N. T., Smyers, S. D., Russell, R. W., Harwit, M., & Melnick, G. 1983, ApJ, 264, 538
Kurucz, R. L. 1979, ApJS, 40, 1
Kutner, M. L., Evans II, N. J., & Tucker, K. D. 1976, ApJ, 209, 452
Kutner, M. L., Guélin, M., Evans II, N. J., Tucker, K. D., & Miller, S. C. 1979, ApJ, 227, 121
Kutner, M. L., Machnik, D. E., Mead, K. N., & Evans II, N. J. 1985, ApJ, 299, 351
Lada, C. J., Elmegreen, B. G., Cong, H.-I., & Thaddeus, P. 1978, ApJ, 226, L39
Langer, W. D., Wilson, R. W., Henry, P. S., & Guélin, M. 1978, ApJ, 225, L139
Lee, T. A. 1968, ApJ, 152, 913
Leung, C. M. 1976, ApJ, 209, 75
Loewenstein, R., et al. 1977, Icarus, 31, 315
Lugten, J. B. 1987, Ph.D. thesis, University of California, Berkeley
Lugten, J. B., Genzel, R., Crawford, M. K., & Townes, C. H. 1986, ApJ, 306, 691
Makinen, P., Harvey, P. M., Wilking, B. A., & Evans II, N. J. 1985, ApJ, 299, 341
Martin, H. M., Sanders, D. B., & Hills, R. E. 1984, MNRAS, 208, 35
Matsuhara, H., et al. 1989, ApJ, 339, L67
Melnick, G., Stacey, G. J., Viscuso, P. J., & Fuller, C. E. 1986, ApJ, 303, 638
Mihalas, D., & Morton, D. C. 1965, ApJ, 142, 253
Münch, G., & Taylor, K. 1974, ApJ, 192, L93
Natta, A., Palla, F., Panagia, N., & Preite-Martinez, A. 1981, A&A, 99, 289
Panagia, N. 1973, AJ, 78, 929
Pankonin, V., & Walmsley, C. M. 1978, A&A, 67, 129
Pankonin, V., Walmsley, C. M., Wilson, T. L., & Thomasson, P. 1977, A&A, 57, 341
Perault, M., Falgarone, E., & Puget, J. L. 1985, A&A, 152, 371
Racine, R. 1968, AJ, 73, 233
Roberge, W. G., Dalgarno, A., & Flannery, B. P. 1981, ApJ, 243, 817
Rubin, R. H. 1968, ApJ, 154, 391
Russell, R. W., Melnick, G., Gull, G. E., & Harwit, M. 1980, ApJ, 240, L99
Russell, R. W., Melnick, G., Smyers, S. D., Kurtz, N. T., Gosnell, T. R., Harwit, M., & Werner, M. W. 1981, ApJ, 250, L35
Savage, B. D. 1975, ApJ, 199, 92
Scalo, J. M. 1986, Fund. Cos. Phys., 11, 1
Scoville, N. Z., & Kwan, J. 1976, ApJ, 206, 718
Stacey, G. J., Geis, N., Genzel, R., Lugten, J. B., Poglitsch, A., Sternberg, A., & Townes, C. H. 1991, ApJ, in press
Stacey, G. J., Smyers, S. D., Kurtz, N. T., & Harwit, M. 1983, ApJ, 268, L99
Stacey, G. J., Viscuso, P. J., Fuller, C. E., & Kurtz, N. T. 1985, ApJ, 289, 803
Stutzki, J., & Güsten, R. 1990, ApJ, 356, 513
Stutzki, J., Stacey, G. J., Genzel, R., Harris, A. I., Jaffe, D. T., & Lugten, J. B. 1988, ApJ, 332, 379
Sullivan III, W. T., & Downes, D. 1973, A&A, 29, 369
Thronson, H. A. 1986, ApJ, 306, 160
Thronson, H. A., Campbell, M. F., & Hoffman, W. F. 1980, ApJ, 239, 533
Tielens, A. G. G. M., & Hollenbach, D. 1985a, ApJ, 291, 722 (TH)
———. 1985b, ApJ, 291, 747
van Dishoeck, E. F., & Black, J. H. 1988, ApJ, 334, 771
Walmsley, C. M. 1975, in H II Regions and Related Topics, ed. T. L. Wilson & D. Downes (New York: Springer), 17
Werner, M. W. 1970, Ap. Letters, 6, 81
Werner, M. W., et al. 1980, ApJ, 242, 601
White, G. J., Sanderson, C., Monteiro, T. S., Richardson, K. J., & Hayashi, S. S. 1990, A&A, 227, 200
Witt, A. N., & Schild, R. E. 1988, ApJ, 325, 837
Wolfire, M. G., Hollenbach, D., & Tielens, A. G. G. M. 1989, ApJ, 344, 770
Wolfire, M. G., Tielens, A. G. G. M., & Hollenbach, D. 1990, ApJ, 358, 116
Wootten, A., Loren, R. B., & Snell, R. L. 1982, ApJ, 255, 160
Wootten, A., Phillips, T. G., Beichman, C. A., & Frerking, M. 1982, ApJ, 256, L5
Wootten, A., Sargent, A., Knapp, G., & Huggins, P. J. 1983, ApJ, 269, 147
Yusef-Zadeh, F. 1990, ApJ, 361, L19
Zuckerman, B., & Ball, J. A. 1974, ApJ, 190, 35